Journal of Zhejiang University-SCIENCE B (Biomedicine & Biotechnology) in press
www.jzus.zju.edu.cn; www.springer.com/journal/11585
E-mail: jzus_b@zju.edu.cn

Research Article

https://doi.org/10.1631/jzus.B2500422

A tumor-stroma interface-on-chip using decellularized lung-tissue-derived hydrogel to investigate alterations in tissue architecture during lung-tumor progression

Aysel SASKARA[1], Yagmur ARSLAN[1,2], Ozlem YESIL-CELIKTAS[1,3,4]✉

[1]*Department of Bioengineering, Faculty of Engineering, Ege University, Izmir, 35100 Turkey*
[2]*Biomechanics section, Department of Mechanical Engineering, KU Leuven, Leuven, 3001, Belgium*
[3]*Translational Pulmonary Research Center (EgeSAM), Ege University, Izmir, Turkey*
[4]*ODTÜ MEMS Center, Ankara, 06530, Turkey*

Abstract: Lung cancer remains a significant global health concern due to frequent late-stage diagnosis. Although intense research efforts are devoted to developing treatment options, the alterations in lung parenchyma are less explored. In this study, we developed an extracellular matrix (ECM)-based hydrogel by decellularizing lung tissue and combining it with gelatin methacrylate (GelMA) to recapitulate stromal tissue and explore ECM remodeling. About 98% of DNA was removed with the optimized decellularization protocol, while collagen and elastin were preserved at 70% and 62%, respectively. Notably, the sulfated glycosaminoglycan (sGAG) content remained nearly unchanged. Lung-cancer cells were embedded in hydrogel containing dlECM (decellularized lung ECM) and GelMA to form a tumor focus, while lung fibroblast cells were seeded around the focus, and lung epithelial cells were layered on top of the hydrogel, forming the tissue construct of the dynamic tumor-stroma interface-on-chip, which was operated for 14 days. Rheological analysis showed that the tumor model exhibited a higher storage modulus (SM, G') (154.7 Pa) compared to the healthy one (108.29 Pa), indicating a stiffer ECM, which was correlated with increased collagen (400.80 μg/mL vs. 218.56) and elastin (2644.40 vs. 1612.07 μg/mL). This contributed to tumor progression through cancer-driven ECM remodeling. In addition, MMP-2 (31.8 ng/mL) and MMP-9 (7.4 ng/mL) levels, which are associated with tumor progression, were significantly elevated on day 7. Our hybrid hydrogel demonstrated the critical role of ECM in lung-cancer progression by revealing biochemical and mechanical changes in the tumor microenvironment (TME); we anticipate that this will provide critical insights into disease progression.

Key words: Organ-on-chip; Decellularized tissue; Hydrogel; Tiissue engineering; Lung tumor stroma interface

Under review

1 Introduction

Lung cancer remains one of the most frequently diagnosed cancers worldwide, posing a significant clinical challenge despite advancements in treatments such as surgery, chemotherapy, and targeted therapies (Herbst et al., 2018; Tao, 2019). The majority of patients are diagnosed at advanced stages, which reduces curability due to the TME and widespread metastasis (Ardalan et al., 2024). Early detection is often challenging. Thus, there is an urgent need for novel clinical models to improve early detection and treatment strategies. Animal models are traditionally used in cancer research; however, ethical concerns, regulatory restrictions, and significant anatomical differences between humans and animals have led researchers to explore alternative models (Esch et

✉ Ozlem YESIL-CELIKTAS, ozlem.yesil.celiktas@ege.edu.tr
Ozlem YESIL-CELIKTAS, https://orcid.org/0000-0003-4509-2212

Received July 20, 2025; Revision accepted Sept. 27, 2025;
Crosschecked xxx. xx, 20xx; Published online xxx. xx, 20xx

© Zhejiang University Press 2025

al., 2015). Among these alternatives, microfluidic systems have demonstrated great potential for simulating cellular microenvironments, enabling the study of cell-cell interactions and disease mechanisms (Yildiz-Ozturk et al., 2021; Kaya et al., 2024). Microfluidic platforms facilitate the mimicry of human lung tissue in controlled environments. This offers a more accurate reflection of cancer cell-environment interactions compared to traditional two-dimensional (2D) cultures (Li et al., 2019).

The extracellular matrix (ECM) is a dynamic three-dimensional (3D) network composed of structural proteins, glycoproteins, and proteoglycans that provides structural support and regulates essential cellular functions, including adhesion, proliferation, migration, and differentiation (Saraswathibatla et al., 2023). ECM components such as collagens, fibronectin, integrins, proteoglycans, laminin, and various growth factors, play critical roles in cell signaling, morphogenesis, and cell-cell interactions (Karamanos et al., 2021). In cancer, ECM composition is altered, with increased expression of fibronectin, laminin, and collagen types I and IV contributing to greater ECM stiffness (Thakor et al., 2020). Additionally, matrix metalloproteinases (MMPs), particularly MMP-2 and MMP-9, are upregulated, leading to ECM remodeling and promoting tumor invasion (Mishra et al., 2012). Studying ECM changes in lung-cancer progression is therefore important for developing early diagnostic tools and targeted therapies (Ferreira et al., 2020). Hydrogels are extensively utilized in tissue engineering due to their ability to replicate ECM properties; this provides a hydrated, porous structure that facilitates cell growth, nutrient diffusion, and waste removal (Blanco-Fernandez et al., 2021; Parvin et al., 2024). Hydrogel formulations based on decellularized tissue have been developed to retain native ECM composition and biomechanical properties, making them highly suitable for tissue-engineering applications (Elosegui-Artola et al., 2023). Various decellularization methods, including physical (freeze-thaw cycles, sonication, etc.), chemical (detergents such as SDS and Triton X-100), and enzymatic (trypsin, DNase, etc.) approaches, are employed to optimize ECM preservation (Wang et al., 2022). While Triton X-100 effectively preserves sGAG and collagen, SDS achieves more efficient cell removal but may cause ECM degradation (Moffat et al., 2022; Das et al, 2020). Hence, it is crucial to optimize decellularization protocols to preserve ECM proteins. Hydrogel formation from decellularized tissue involves solubilizing fibrillar proteins in an acid-pepsin solution, followed by gelation under physiological conditions, which allows precise control over mechanical and biochemical properties (Saldin et al., 2017).

dECM derived from bovine lung tissue has been studied due to its availability and biochemical similarity to human ECM. Several studies have reported the decellularization of bovine lung tissue to develop scaffolds for tissue engineering. For instance, Kusoglu et al., 2023 compared different decellularization methods and demonstrated that bovine lung ECM preserves key biochemical components and provides reproducible mechanical properties, supporting its use as an alternative to human lung ECM. Similarly, Ozdinc et al., 2023 developed and characterized bovine lung dECM hydrogels, demonstrating that optimized protocols yield scaffolds with distinctive viscoelastic and biochemical features that enhance their translational potential. In this concept, we decellularized bovine lung tissue by optimizing a combination of chemical, biological, and physical methods. The tissue was then characterized with respect to DNA content, total protein, collagen, sGAG, and elastin levels, along with SEM imaging to evaluate ECM morphology. The decellularized lung tissue was processed into a pre-gel solution and combined with GelMA to recapitulate the lung microenvironment (LME). A tumor focus was formed with human lung carcinoma cells, surrounded with human lung fibroblasts embedded in GelMA-dlECM hydrogel, while human bronchial epithelial cells were seeded on top of the hydrogel to form the tumor-stroma interface-on-chip platform, which was operated for 14 days. Finally, we investigated the changes in ECM associated with lung-cancer progression by biochemical and rheological analysis.

Unedited

2 Material and methods

2.1 Cell culture

Human bronchial epithelium (BEAS-2B, ATCC, USA), human lung fibroblasts (CCD-34Lu, ATCC, USA) and human lung carcinoma cells (A549, ATCC, USA) were cultured in Dulbecco's Modified Eagle Medium/Nutrient Mixture F-12 (DMEM-F12) cell culture medium supplemented with 10% (volume fraction) FBS, 1% (volume fraction) L-glutamine (200 mmol/L), 0.5% (volume fraction) penicillin/streptomycin (100U/100 mg/ml), 0.5% Gentamicin (10 mg/mL), and 1% non-essential amino acid (100x). Cells were cultured in a T-flask with filter cap in a humidified incubator in a 5% CO_2 and 95% air atmosphere at 37 °C. Cell passaging was performed every week using 0.05 % (volume fraction) trypsin/ethylenediaminetetraacetic acid (EDTA) when it reached confluence. All reagents were supplied by Sigma-Aldrich (UK).

2.2 Decellularization of lung tissue

Fresh bovine lungs were obtained from a farm (Konya, Turkiye). Lung tissues were washed with Phosphate Buffered Saline (PBS, Capricorn Scientific, Germany) containing 1% (volume fraction) Amphotericin B (Biochrom, Germany) and 1% (volume fraction) Penicillin-Streptomycin (P/S) (Sigma-Aldrich, UK) and stored at -80° C until further use. Tissues were then dissected approximately 1 cm^3 from different parts of the lung, including the bronchi and bronchioles. The sliced lung tissues were decellularized with a combination of chemical, biological, and physical methods. Prior to decellularization, sliced lung tissues were washed with distilled water for 1 hour (h) and washed afterwards with distilled water containing 1% (volume fraction) Amphotericin B and 1% (volume fraction) Penicillin-Streptomycin at room temperature (RT) overnight to remove blood and impurities. After antibiotic treatment, tissues were rinsed with distilled water for 2 h. In the first protocol (P1), lung tissues were treated with 0.5% (volume fraction) Triton X-100 (Sigma-Aldrich, UK) for 24 h. Tissues were then washed with distilled water for 2 h and subsequently exposed to a second 24-h treatment of 0.5% (volume fraction) Triton X-100. In the second protocol (P2), lung tissues were treated with 0.1% (volume fraction) Triton X-100 for 24 h. Then, they were washed with distilled water for 2 h, and 0.5% (volume fraction) Sodium Dodecyl Sulfate (SDS) (ABT Laboratory Industry, Turkey) was applied for 24 h. Detergent residues were removed by washing with distilled water between each treatment. Then, the tissues were washed with 0.1% (volume fraction) peracetic acid (Merck, 433241, Germany) in 4% (volume fraction) ethanol for 2 h to remove the cellular components remaining in the tissues and treated with 1X PBS to regulate the pH after peracetic acid treatment. Lastly, the tissues were rinsed with distilled water for 2 h and stored at -20 °C until lyophilized. Tissues were then lyophilized for 2 days. All decellularization agents were applied under room temperature (RT) with continuous shaking at 150 r/min on an orbital shaker.

Uncorrected

2.3 Characterization of decellularized lung tissue

2.3.1 DNA analysis and agarose gel electrophoresis

We quantified the DNA content in both native and decellularized lyophilized lung tissue using the DNeasy Blood & Tissue Kit (Qiagen, 69504, Germany). The DNA concentration (ng DNA/mg dry weight) was measured using a Nanodrop spectrophotometer, while DNA fragment length was assessed via 1% (g/mL) agarose gel electrophoresis.

2.3.2 Protein content

Total protein content in the native and decellularized lung tissue was quantified using the bicinchoninic acid assay (Pierce™ BCA Protein Assay Kit, 23225, Thermo Scientific, USA) following extraction with RIPA lysis buffer (Thermo Scientific, 89901, USA). The collagen content was determined using the Sircol Collagen Assay Kit (Biocolor Ltd, S1111 Std, UK) following digestion in 0.5 mol/L acetic acid with 0.1 mg/mL pepsin at 4 °C for 24 h. The sGAG content was analyzed using the Blyscan Glycosaminoglycan Assay Kit (Biocolor Ltd, B1000, UK) after tissue extraction with a papain extraction reagent (containing papain, EDTA disodium salt, L-cysteine hydrochloride, and sodium acetate) at 65 °C for 3 h. The collagen content was determined using the Sircol Collagen Assay Kit (Biocolor Ltd, S1111 Std, UK) following digestion in 0.5 mol/L acetic acid with 0.1 mg/mL pepsin (Sigma-Aldrich, P7012, UK) at 4 °C for 24 h. Elastin quantification was performed using the FASTIN Elastin Assay Kit (Biocolor, F2000, UK) after 0.25 mol/L oxalic acid treatment at 90 °C for 1 h. All analyses were performed according to the manufacturer's instructions. All data were quantified as μg/mg dry weight.

2.3.3 Scanning electron microscopy (SEM)

SEM imaging was conducted at the Ege University Central Research Test and Analysis Laboratories Application and Research Center (EGE MATAL) to evaluate morphological changes before and after decellularization. Lyophilized samples were sectioned, mounted onto carbon tape, and sputter-coated with a 10 nm gold layer (Leica EM ACE600). We performed imaging using SEM at an acceleration voltage of 7.5 kV with a secondary electron detector (SE).

Unedited

2.4 Hydrogel preparation

2.4.1 Production of dlECM pre-gel solution

We sterilized the lyophilized decellularized lung tissue with ethylene oxide and mechanically fragmented it using a sterile scalpel to enhance solubilization. The dlECM was then enzymatically digested in a 1 mg/mL pepsin solution in 0.01 mol/L HCl under constant agitation for 48 h at RT, yielding two stock solutions of 10 mg/mL and 20 mg /mL. 10 mg/mL hydrogel concentration was used for further applications within this study due to it’s homogeneus structure compared to other one. We removed the insoluble residues via centrifugation at 1500 r/min for 10 min, collected the solubilized supernatant, and stored it at -20 °C as a stock solution. Prior to hydrogel formation, the pH and ionic strength of the pre-gel solution were adjusted using 0.1 mol/L NaOH and 10X PBS, respectively.

2.4.2 Preparation of methacrylated gelatin (GelMA) prepolymer solution

GelMA was synthesized according to the protocol reported by Cakmak et al., 2022. A 10% (0.1 g/mL) gelatin (Sigma-Aldrich, Cat No: 62500, UK) solution was prepared by stirring gelatin in PBS at 50 °C until completely dissolved. Subsequently, methacrylic anhydride (Sigma-Aldrich, Cat No: 276685, UK) was added dropwise and the reaction was continued for 2 h. After that, the solution was diluted with an additional PBS and further stirred for 10 min. The solution was then subjected to dialysis (14,000 MW cut-off) against distilled water at 40 °C for 5 d with continuous stirring. Post-dialysis, the GelMA solution was filtered through a 0.45 μm filter, transferred to storage tubes, and sequentially frozen at -80 °C before lyophilization for 72 h. We prepared GelMA hydrogel by dissolving 5% (g/mL) GelMA and 1% (g/mL) Irgacure 2959 photoinitiator (2-hydroxy-4’-(2-hydroxyethoxy) -2-methylpropiophenone (Irgacure2959, Sigma-Aldrich, Dorset, UK) separately in DMEM-F12 basal medium

at 70 °C for 30 min. These solutions were combined as a prepolymer solution, mixed at 40 °C for 15 min, and sterilized via filtration through a 0.22 μm filter (Cakmak et al., 2022).

2.4.3 Optimization of GelMA-dlECM hydrogel formulation

To prepare an optimized composite hydrogel, we mixed dlECM pre-gel solution with 5% (g/mL) GelMA prepolymer solution at different volume ratios. Prior to this, we embedded A549 human lung carcinoma cells and CCD-34Lu human lung fibroblasts (1:1 ratio) with a total concentration of 10^6 cells/mL in hydrogels with different volume ratios (i.e., 100% GelMA, 75% GelMA–25% dlECM, 62.5% GelMA–37.5% dlECM, and 50% GelMA–50% dlECM) (volume fraction). Photocrosslinking of 3D hydrogels was performed for 30 s under ultraviolet (UV) light (800 mW/cm^2) (Omnicure, Canada). Cell viability was then evaluated using the Cell Counting Kit-8 (WST-8/CCK8) assay (ab228554, Abcam, USA). Briefly, 10% (volume fraction) CCK8 solution was added to the fresh culture medium, and the hydrogels were incubated for 4 h at 37 °C and 5% CO^2. After incubation, we measured the absorbance at 460 nm using a microplate reader.

2.5 Recapitulating lung-tumor focus in the tumor-stroma interface-on-chip

The platform consisted of a tissue chamber 8 mm × 15 mm × 3 mm in size (Width × Length × Height), produced using polymethylmethacrylate (PMMA) molds fabricated by laser cutting (VLS2.30 system Universal Laser). Biocompatible and oxygen-permeable polydimethylsiloxane (PDMS) solution (PDMS, SYLGARD™ 184, Germany) was obtained by mixing the PDMS elastomer base and curing agent at a 10:1 (weight fraction) ratio. Then, the PDMS solution was poured into the molds to fabricate tissue chamber and reservoir, degassed under a vacuum pump, and cured at 60 °C overnight. After curing, the PDMS was peeled off the molds, and all components were sterilized with ethylene oxide.

Uncited

We established three experimental groups on the tumor-stroma interface-on-chip platform to evaluate lung-cancer-induced ECM alterations under dynamic conditions: *(I) Cancer Group, (II) Healthy Group, and (III) Control Group.*

Group I: Cancer Group. A549 cells with a concentration of 1x10^6 cells/mL were embedded in GelMA-dlECM hydrogel to mimic the TME of lung tissue. The hydrogel-cell suspension was homogenized and dispensed as 30 μL droplets within a PDMS chamber, followed by UV crosslinking to induce gelation to form a tumor focus. To enable tracking of A549 cell migration, cells were pre-labeled with Hoechst solution (1 μg/mL, Sigma-Aldrich, UK) before encapsulation. Subsequently, we embedded CCD-34Lu human lung fibroblasts with a concentration of 5×10^5 cells/mL in GelMA-dlECM hydrogel to simulate the microenvironment surrounding the tumor structure. The fibroblast-embedded hydrogel was placed into the chamber and crosslinked via UV exposure. Following fibroblast encapsulation, BEAS-2B human bronchial epithelial cells with a concentration of 1×10^6 cells/mL were seeded onto the top layer of the hydrogel construct to recapitulate the epithelial barrier. The epithelial and fibroblast cell-concentration ratio was maintained at 1:2, as described in a previous paper (Saygili et al., 2023). To facilitate the localization of cell populations, CellTracker Green (20 μM) and CellTracker Red (10 μM) fluorescent dyes (Life Technologies, USA) were used for epithelial and fibroblast cells, respectively.

Group II: Healthy Group. The healthy LME was reconstructed using a similar methodology without cancer cells. Thus, CCD-34Lu fibroblasts with a concentration of 5×10^5 cells/mL were embedded in GelMA-dlECM hydrogel, cast into the PDMS chamber, and crosslinked via UV exposure. Subsequently, BEAS-2B epithelial cells with a concentration of 1×10^6 cells/mL were seeded on top of the hydrogel surface at a fibroblast- and epithelial-cell concentration ratio of 1:2.

Group III: Control Group. The control group was designed to evaluate the effects of the hydrogel microenvironment in the absence of cellular components. For this purpose, GelMA-dlECM hydrogel was cast into the PDMS reservoir and subjected to UV crosslinking.

After the seeding of each group, the culture medium was supplemented in the upper reservoir, and the platform was incubated under culture conditions (37 °C, 5% CO_2) for 14 days on a rocker system. In our model, interstitial blood flow was emulated using a rocking platform at 0.1 r/min (1 cycle per 600-second period), which generated a bidirectional ~ 0.1 μm/s fluid flow to emulate the interstitial blood-flow range of the TME reported in the literature (Rahman et al., 2024; Evje et al., 2019; Munson et al., 2014). We estimated interstitial flow rate using Darcy's law. Considering the chamber geometry (*height*=3 mm, *width*=8 mm, *length*=15 mm), rocker tilt angle ($\theta = 8°$), fluid density (ρ = 1009 kg/m³), dynamic viscosity (μ = 0.00093 Pa·s), and hydrogel permeability ($k = 10^{-13}$ m²), the interstitial velocity is given by $v = (k/\mu)\nabla P$ and $\nabla P = \rho g \sin\theta$. Using the values, the resulting interstitial velocity is $v \approx 0.1$ μm/s (Poon et al., 2012; Miri et al., 2018)

2.6 Evaluating the effects of tumor focus on the lung microenvironment

2.6.1 Biochemical analysis

We quantified the levels of matrix metalloproteinases, which play a key role in ECM remodeling in lung-cancer progression, using MMP-2 and MMP-9 ELISA kits (FineTest, China). These analyses were conducted on the 7th and 14th days of culture to assess matrix degradation in the hydrogel. To further investigate the biochemical impact of cancer on ECM, we determined total protein content in each group using the Pierce™ BCA Protein Assay Kit, following protein extraction with RIPA lysis buffer. Collagen content was quantified via the Sircol Collagen Assay Kit after enzymatic digestion in 0.5 mol/L acetic acid containing 0.1 mg/mL pepsin at 4 °C for 24 h. Elastin content was analyzed using the FASTIN Elastin Assay Kit following hydrolysis with 0.25 mol/L oxalic acid at 90 °C for 1 h. All data were quantified as μg/mL.

2.6.2 Rheological analysis

To investigate the mechanical alterations in ECM induced by cancer, rheological characterization was performed at the Katip Celebi University Central Research Laboratories Application and Research Center. Key rheological parameters, including complex viscosity, SM, and loss modulus (LM, G"), were assessed. Hydrogel samples were placed under a rheometer plate (Discovery HR 30, TA Instruments, USA), and the probe was lowered to a predetermined gap height (500–1000 μm). For shear-modulus evaluation, we conducted frequency sweep tests in the range of 0.1 Hz to 100 Hz, and determined the optimal frequency to be 0.5 Hz within the linear region. Subsequently, viscosity, LM and SM measurements were recorded at 0.5 Hz, 1% strain, and 37 °C over a duration of 10 minutes.

2.7 Statistical analysis

Statistical analysis was performed using GraphPad Prism 8.3.0. All experiments were performed at least three times. Data were expressed as mean±standard deviation (n=3). Data were analyzed by two-way ANOVA with Tukey's multiple comparison test and Student's t-test (ns: non-significant; $P > 0.05$, $^{*}P < 0.05$, $^{**}P < 0.01$, $^{***}P < 0.001$, $^{****}P < 0.0001$).

Unedited

3 Results and discussion

3.1 Decellularization and characterization of lung tissue

Numerous strategies have been proposed to recapitulate the structural and biochemical properties of the native ECM. One approach involves using both synthetic and naturally derived biomaterials. Synthetic materials offer tunable mechanical properties and reproducibility. However, they often lack the complex biochemical cues, and structural intricacies present in native ECM, which are essential for guiding cell behavior. Naturally derived materials, on the other hand, provide better mimicry of the ECM's biochemical composition, and support cellular functions such as adhesion, proliferation, and organization (Devamoglu et al., 2025). On the other hand, their compositional simplicity and batch-to-batch variability limit broader applicability. To overcome these limitations, decellularized tissue-derived matrices have emerged as a promising alternative due to their preserved biochemical complexity and structural fidelity; they offer a physiologically relevant platform that better simulates both the LME and TME. Unlike single-component natural or synthetic materials, decellularized ECM (dECM) preserves the native tissue's structural complexity and biochemical composition, allowing for the reconstruction of a microenvironment that precisely approximates *in vivo* conditions. This makes it particularly valuable for studies that require physiologically accurate models to investigate cell-matrix interactions, tissue-specific responses, and disease mechanisms under near-native conditions (Wang et al., 2024). The decellularization process, however, requires precise optimization to balance cellular content removal while preserving ECM integrity. Complete elimination of all cellular components from the tissue is not feasible, yet two criteria have been proposed as the gold standard to prevent a proinflammatory response yielding cell viability: (i) the amount of DNA should be <50 ng DNA/mg dry weight, and (ii) the length of DNA fragments should be <200 bp (Yaldiz et al., 2021a).

In this study, we carried out consecutive steps to optimize decellularization (**Fig. 1a**) and endeavored to establish a basis for further protocol development. We applied two distinct decellularization protocols (**Fig. 1b**). The first protocol (P1) exclusively utilized Triton X-100, which is known for being gentler on ECM and having lower residual toxicity, making it suitable for soft-tissue applications (Fu et al., 2016). P1 resulted in insufficient DNA clearance (906.32±16.1) ng/mg dry weight), indicating its inadequacy for nuclear content removal. To en1hance cell removal efficiency, the second protocol (P2) incorporated both Triton X-100 and SDS at optimized concentrations (0.5% SDS and 0.1% Triton X-100). SDS, an ionic detergent, is particularly effective in decellularizing dense and highly vascularized tissues such as cartilage, tendons, lungs, liver, and vascular grafts (Inci et al., 2020). Incorporating SDS into the protocol significantly enhanced decellularization efficiency and, reducing DNA content (55.53±2.8) ng DNA/mg dry weight), which met the proposed threshold criteria. This represented a 98% reduction in DNA relative to native tissue (3057.88±391.6) ng/mg), demonstrating the effectiveness of the dual-detergent strategy (**Fig. 1c-e).** Additionally, the consistency between independent batches emphasizes the reproducibility of P2 and addresses one of the major drawbacks of natural biomaterials such as Matrigel. Despite its widespread use, Matrigel's undefined composition and origin in malignant tissue restrict its utility in reproducible and clinically relevant models (Hocevar et al., 2021; Kleinman and Martin, 2005). DNA contents of the first and second batches (54.98±2.1) ng DNA/mg dry weight and (59.6±0.6) ng DNA/mg dry weight, respectively) highlight the reliability of the protocol **(Fig. 1f)**. Supporting these findings, agarose gel electrophoresis demonstrated clear banding differences between native and decellularized samples. DNA fragmentation below 200 bp in the decellularized samples further validates the efficacy of the optimized protocol in minimizing residual nuclear material (**Fig. 1g**) and meets the second criterion for minimizing residual DNA, reducing immunogenicity. In addition, SEM images of both native **(Fig. 1h, i)** and decellularized **(Fig. 1h, ii)** lung tissue confirmed that nuclear material was eliminated, and the ECM ultrastructure remained intact post-decellularization, preserving key characteristics necessary for cell adhesion and tissue remodeling.

Uncorrected

(a)

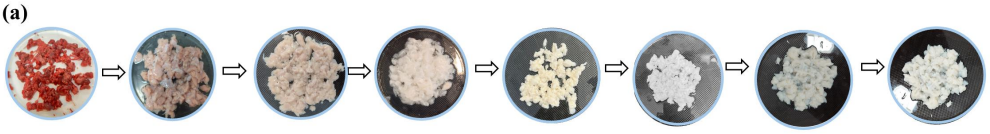

(b)

	30 min*3 times	2 hours	Overnight	24 hours	24 hours	2 hours	30 min	2 hours
P1	Freeze-Thaw	Distilled Water	1% Antibiotic	0,5% Triton-X-100	0,5% Triton-X-100	0,1% Peracetic Acid	PBS	Distilled Water
P2	Freeze-Thaw	Distilled Water	1% Antibiotic	0,1% Triton-X-100	0,5% SDS	0,1% Peracetic Acid	PBS	Distilled Water

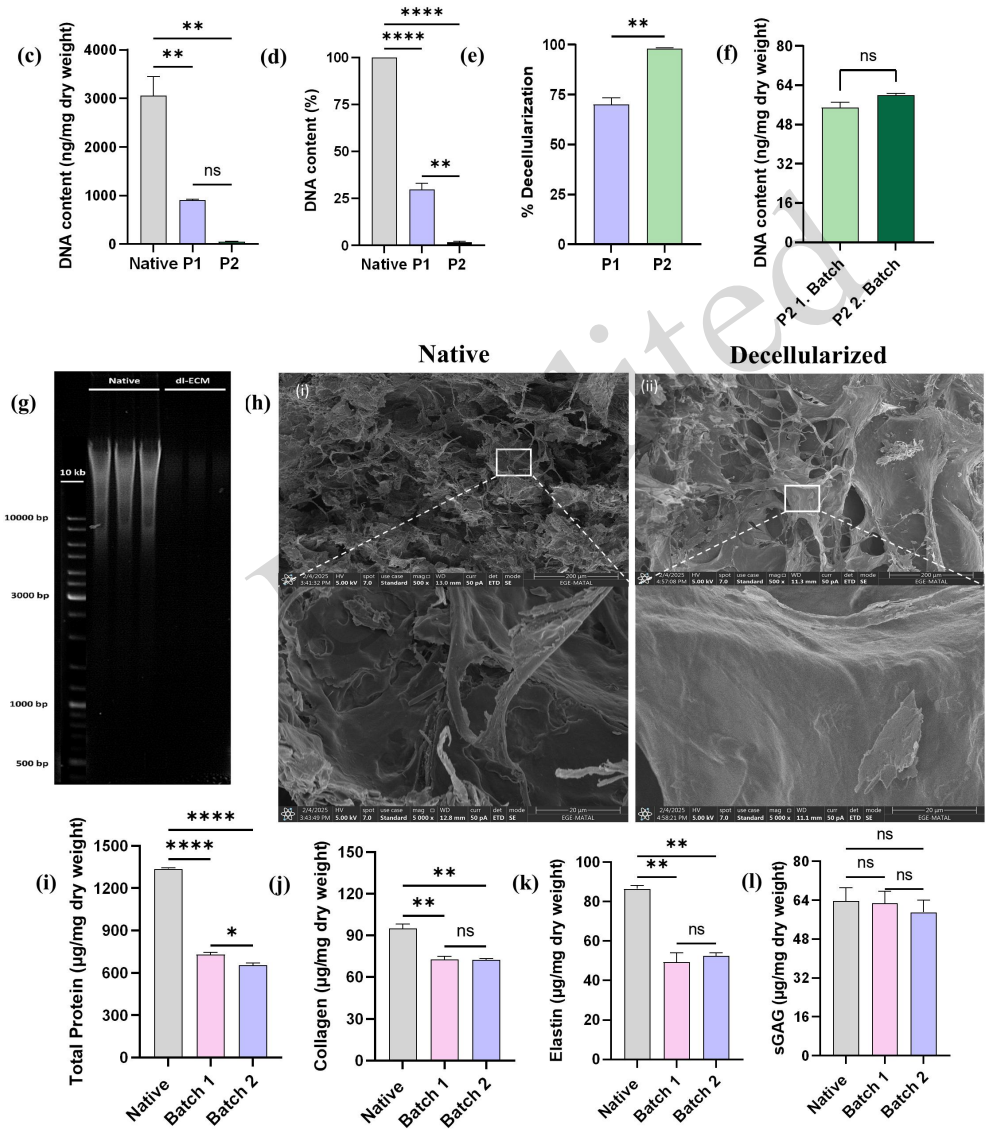

Fig. 1. Decellularization and characterization of bovine lung tissue. (a) The consecutive steps corresponding to each of the treatments in the decellularization protocol (b) Decellularization protocols, (c) DNA content (ng/mg dry weight) and (d) DNA content as a percentage (%) of native and decellularized lung tissue, (e) decellularization success as a percentage (%), (f) DNA content of different batches of decellularized lung tissue, (g) Gel electrophoresis images of native and decellularized tissue, (h) SEM images of (i) native and (ii) decellularized tissue. (500x scale bar: 200 µm, 5000x scale bar: 20 µm) indicating morphological structure, (i) total protein, (j) collagen, (k) elastin and (l) sGAG content of the native and decellularized tissue (batches 1 and 2). Data are expressed as mean±standard deviation (SD) (n=3). Error bars represent sd (ns, no significance, $^{*}P$<0.05, ** P<0.01, *** P<0.001, $^{****}P$<0.0001). P1 represents first protocol, P2 represents second protocol.

Decellularized ECM retains tissue-specific components, including proteoglycans as well as structural and functional proteins, all of which are essential for maintaining the biochemical and mechanical properties of native tissue (Yaldiz et al., 2021b). One critical aspect following decellularization is ensuring minimal loss of key proteins, as their decrease may affect the functional integrity of the scaffold (Ohata and Ott, 2020; O'Neill et al., 2013). To address this, we quantified total protein, collagen, elastin, and sGAG contents. Following decellularization, approximately 50% of the total proteins were preserved in both batches (730.44±15.7 μg/mg and 645.05±15.7 μg/mg for Batch 1 and Batch 2, respectively) compared to native lung tissue (1336.69±8.8 μg/mg dry weight) (**Fig. 1i**). This indicated the effectiveness of our protocol in maintaining essential protein components. Collagen, a primary structural component of the ECM responsible for scaffold integrity (Valdoz et al, 2021), was retained at around 70% in both batches of decellularized lung tissue (73.56±2.1 μg/mg and 72.42±1.1 μg/mg for Batch 1 and Batch 2, respectively) (**Fig. 1j**). Elastin, which contributes to elasticity and mechanical resilience (Trebacz and Barzycka, 2023), was preserved at approximately 62% in both batches (49.41±4.8 μg/mg and 52.43±1.6 μg/mg, respectively) (**Fig. 1k**). Lastly, the sGAG content, vital for hydration and biochemical signaling within the ECM (Gilbert et al., 2021), was nearly completely retained, with preservation close to 100% in both batches (62.76±4.9 μg/mg and 59±4.9 μg/mg, respectively) (**Fig. 1l**). These findings confirm that the decellularization process effectively preserves key ECM proteins and exhibits minimal batch-to-batch variability. The high degree of preservation supports the potential of the derived scaffold as a starting point for development of further hydrogels (Kusoglu et al., 2023).

3.2 Hydrogel synthesis from decellularized lung tissue and optimization of the GelMA-dlECM ratio

Hydrogel formation from decellularized lung tissue is primarily driven by a collagen-based self-assembly mechanism (Zhu et al., 2018). To optimize hydrogel formulation, gelation efficiency was assessed at two ECM concentrations: 10 mg/mL and 20 mg/mL. The 10 mg/mL hydrogel exhibited homogeneous mixing but remained in a liquid-like state. On the other hand, the 20 mg/mL hydrogel displayed heterogeneity, with tissue particles failing to fully integrate into the gel matrix (**Fig. S1**). To address this latter issue, we first ground the tissue into a fine powder to enhance homogeneity; however, instead of dispersing uniformly, the particles aggregated into clusters. Replacing old pepsin with fresh one and preparing a fresh HCl solution did not resolve the heterogeneity problem. Next, we tried incorporating GelMA into the dlECM hydrogel to improve mechanical stability and homogeneity (**Fig. 2a**). GelMA, a semi-synthetic hydrogel derived from gelatin and functionalized with methacryloyl groups, enhances gelation kinetics and mechanical properties while preserving biocompatibility and bioactivity (Lim et al., 2019; Yue et al., 2015). A range of GelMA–dlECM ratios was evaluated to determine optimal conditions for cell-culture applications (**Fig. 2b**). After 14 days of incubation, cell-viability assays indicated that the 75% GelMA-25% dlECM hydrogel provided the most favorable conditions for cell proliferation with the highest absorbance value of 0.26 (**Fig. 2c)**. This result was corroborated by fluorescence imaging, which showed active proliferation of BEAS-2B (green) and CCD34-Lu (red) cells on the hydrogel surface (**Fig. 2d**).

Unedited

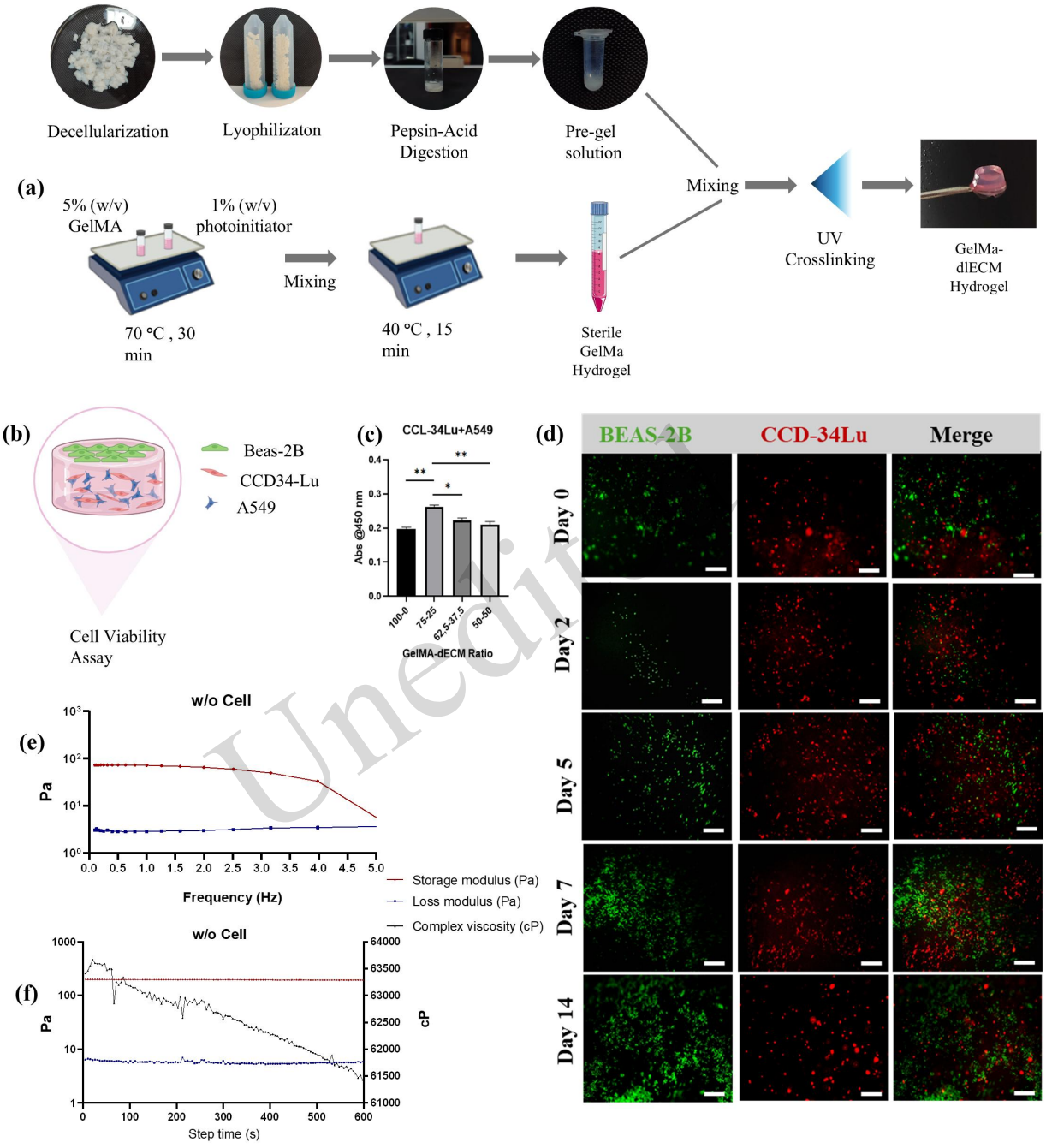

Fig. 2. Development of GelMA-dlECM hydrogel formulation. (a) Step-by-step GelMA-dlECM hydrogel formation. (b) Schematic representation of cell viability assay on lung-cancer, epithelial, and fibroblast cells in dlECM-GelMA hydrogel, (c) Viability of cells in different volume ratios of dlECM and GelMA, (d) CellTracker images of BEAS-2B and A549 cells (Scale bar: 100 μm), (e) Frequency sweep plot of GelMA-dlECM hydrogel and (f) Rheological analysis of GelMA-dlECM hydrogel). Data are expressed as mean±standard deviation (SD) (n=3). Error bars represent standard deviation, sd (ns, no significance, *P< 0.05, **P< 0.01, ***P< 0.001, ****P< 0.0001). w/o cell represents cell-free hydrogel.

Additionally, we performed a frequency sweep analysis, operated at 0.5 Hz within the linear range, to determine the optimal frequency for rheological analysis (**Fig. 2e**). Then, we measured the SM and LM of the hydrogel under 1% strain at 0.5 Hz and 37 °C for 10 minutes. The LM and SM values were 5.6 Pa and 198.89 Pa,

respectively (**Fig. 2f**). These values indicate a predominantly elastic behavior, consistent with the gel's capacity to provide mechanical support for 3D cell culture. Importantly, the value observed for the GelMA–dlECM hydrogel falls within the reported range of native lung stromal tissues under physiological conditions; the tissues generally exhibit storage modulus in the range of ~100–300 Pa, depending on anatomical location and measurement parameters (Phogat et al., 2023). Therefore, the rheological properties of the optimized hydrogel closely recapitulate the mechanical environment of lung parenchyma, supporting its applicability for LME modeling. The relatively LM observed is also a desirable characteristic for mimicking soft-tissue mechanics while allowing adequate structural integrity for *in vitro* experimentation.

3.3 Recapitulating lung-tumor focus in the tumor-stroma interface-on-chip platform

To construct a physiologically relevant TME, we developed a biofabricated model using a hydrogel consisting of 75% GelMA and 25% dlECM. A549 cells were encapsulated as a central tumor droplet, while surrounding stromal regions were populated with CCD-34Lu lung fibroblasts suspended in the same hydrogel composition. To mimic the epithelial barrier, BEAS-2B cells were subsequently seeded onto the upper surface **(Fig. 3a**). Hydraulic tightness was ensured by stabilizing the PMMA layers at the top and bottom of the platform with screws and bolts. The platform was then placed on a rocker to emulate interstitial blood flow (**Fig. 3b**). Interstitial flow in tumor tissues is reported to be in the range of 0.01 - 1 μm/s in different cancer types. We estimated the flow rate using Darcy's law. The resulting interstitial velocity of our model was $v \approx 0.1$ μm/s, consistent with the reported values in the literature (Rahman et al., 2024). After 14 days of culture, cell-tracked images revealed significant tumor-cell invasion from the primary tumor site into the surrounding microenvironment (**Fig. S2**). Notably, A549 cells (blue) demonstrated invasive behavior, migrating outward from the tumor focus on day 2 and reaching a maximum on day 14 (**Fig. 3c**). In addition, proliferations of BEAS-2B (green) and CCD34-Lu (red) cells were evident in the healthy model, confirming the platform's capability to support cell growth and interaction within the LME.

Uncited

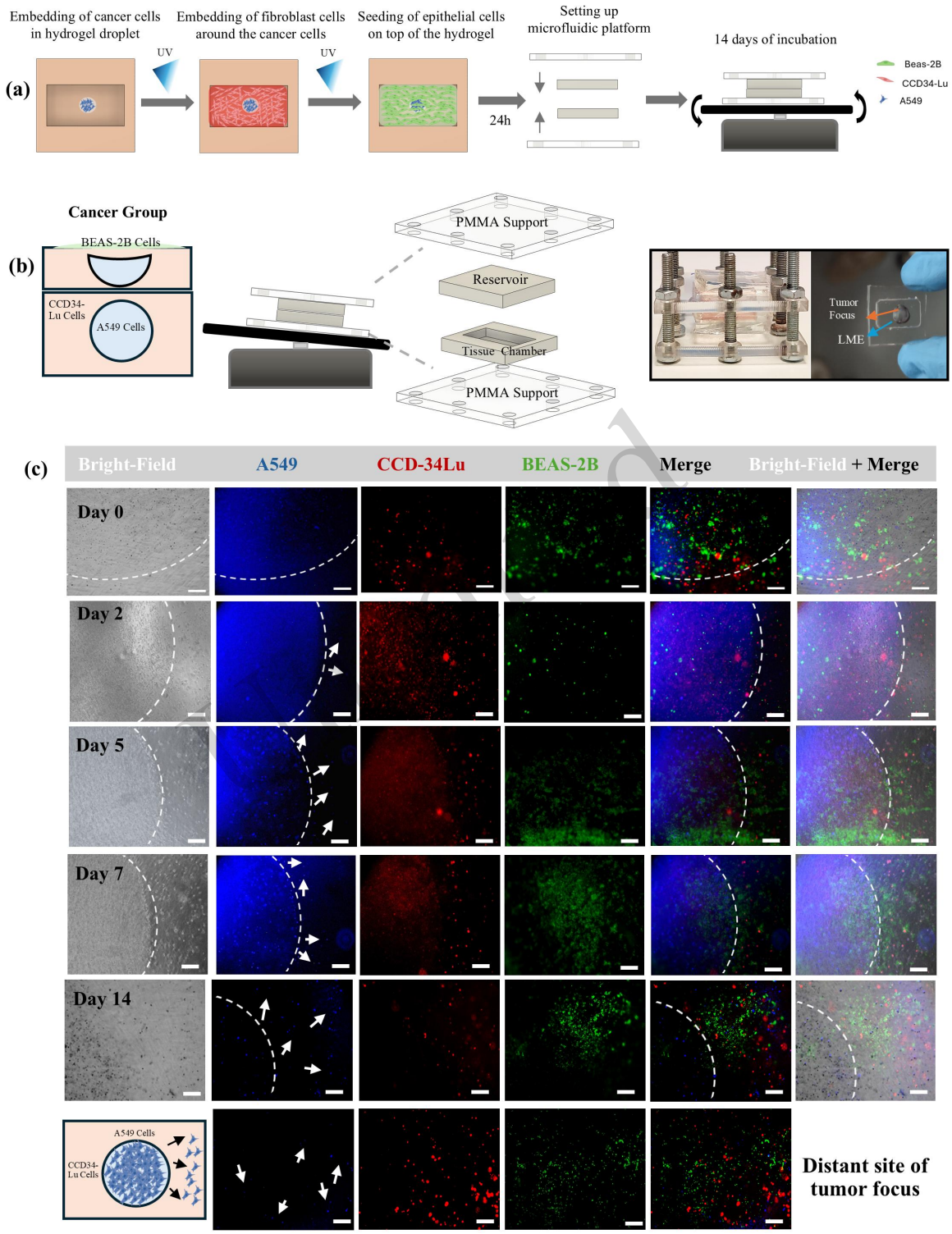

Fig. 3. Recapitulation of lung cancer in the tumor-stroma interface-on-chip platform. (a) Schematic representation of tumor-model development, (b) Schematic representation of the lung-cancer model in the on-chip platform, and layers of the platform and macroscopic image of the tumor-stroma interface-on-chip. (c) CellTracker images of the tumor model in the on-chip platform**.** Dashes indicate droplet structure. (Scale bar: 100 μm). To enable tracking of lung-cancer-cell migration, A549 cells were pre-labeled with Hoechst solution. Epithelial (BEAS-2B) and fibroblast (CCD34-Lu) cells were pre-labeled with CellTracker Green and CellTracker Red fluorescent dyes, respectively.

The preserved biochemical stimulations and tissue-specific matrix components in dECM provide native signaling environments that promote more physiologically relevant responses, such as improved invasion, proliferation, and ECM remodeling. Prior studies have demonstrated that GelMA, while structurally supportive, lacks many of the biochemical compounds (such as proteins and growth factors) found in native ECM. Therefore, the use of a hybrid GelMA-dECM system likely offers advantages not only in recapitulating the tumor-stroma interface, but also in supporting cell proliferation, mechanical stability, and biochemical functionality (Edgar-Vilar et al., 2025; Kort-Mascort et al., 2021). One of the key characteristics of the ECM is its dynamic nature: ECM, cells, and their surrounding microenvironment continuously modify their mechanical properties to adapt and respond to various stimulus. These adaptations facilitate diverse cellular responses, particularly in cell-cell and cell-ECM interactions (Xie et al., 2023). The ECM itself is a porous biopolymer network composed of fibrous proteins such as collagen, elastin, fibronectin, and laminin (Sicari et al., 2014). Its dynamic properties are largely influenced by alterations in protein composition, which directly impact its rheological behavior. Fibrous proteins play a crucial role in regulating tissue elasticity and tensile strength, as well as mediating cell adhesion and tissue development. Collagen is the most abundant fibrous protein in the ECM; the increase in tissue collagen levels promotes tumor progression (Fanjul-Fernández et al., 2013).

Elastin, another key fibrillar protein, is insoluble and strongly associated with tissue recoil following mechanical stretching, due to its highly dynamic 3D structure. Damage to elastin leads to an increased synthesis of elastin-like and elastin-derived peptides, which has been linked to the promotion of tumor progression (Wang et al., 2020). In line with these observations, we conducted rheological analysis of our hydrogel constructs after 14 days of incubation. Since the temperature was kept constant, no significant changes in the moduli were observed over time. Initially, we performed a frequency sweep analysis to determine the optimal frequency for measurements **(Fig. 4a-b)**, and identified 0.5 Hz within the linear range as ideal. Subsequently, groups were compared under 1% strain at 0.5 Hz and 37 °C for 10 minutes. The SM was found to be higher in the tumor model (154.7 Pa) than in the healthy model (108.29 Pa), indicating matrix stiffening consistent with tumor progression **(Fig. 4c-d)** (Firatligil-Yildirir et al., 2024). The LM, which reflects the viscous and elastic response of the hydrogel (Oyen, 2014), was also elevated in the tumor model (4.8 Pa) compared to the healthy model (2.6 Pa). The highest G′ and G″ values were recorded in the cell-free hydrogel (198.89 Pa and 5.6 Pa, respectively), suggesting that cellular activity contributes to ECM degradation and remodeling. The tumor model, which exhibited intermediate stiffness and viscoelasticity, reflects a microenvironment undergoing both matrix breakdown and localized deposition of fibrotic ECM components due to tumor-associated remodeling (Mao et al., 2023). To further elucidate the viscoelastic profile, the loss tangent (tan δ), defined as the ratio of G″ to G′, was calculated. All models, including tumor (0.04), healthy (0.03), and cell-free (0.03), displayed tan δ values below 0.1, confirming predominantly elastic, solid-like behavior with minimal energy dissipation (Bartnikowski et al., 2015). Additionally, viscosity measurements revealed a time-dependent decrease in all groups, with the highest value in the cell-free model (61426.9 cP), followed by the cancer (42928 cP) and healthy models (28118.8 cP), further supporting the concept that cellular presence characterizes ECM remodeling and mechanical softening.

Uncorrected

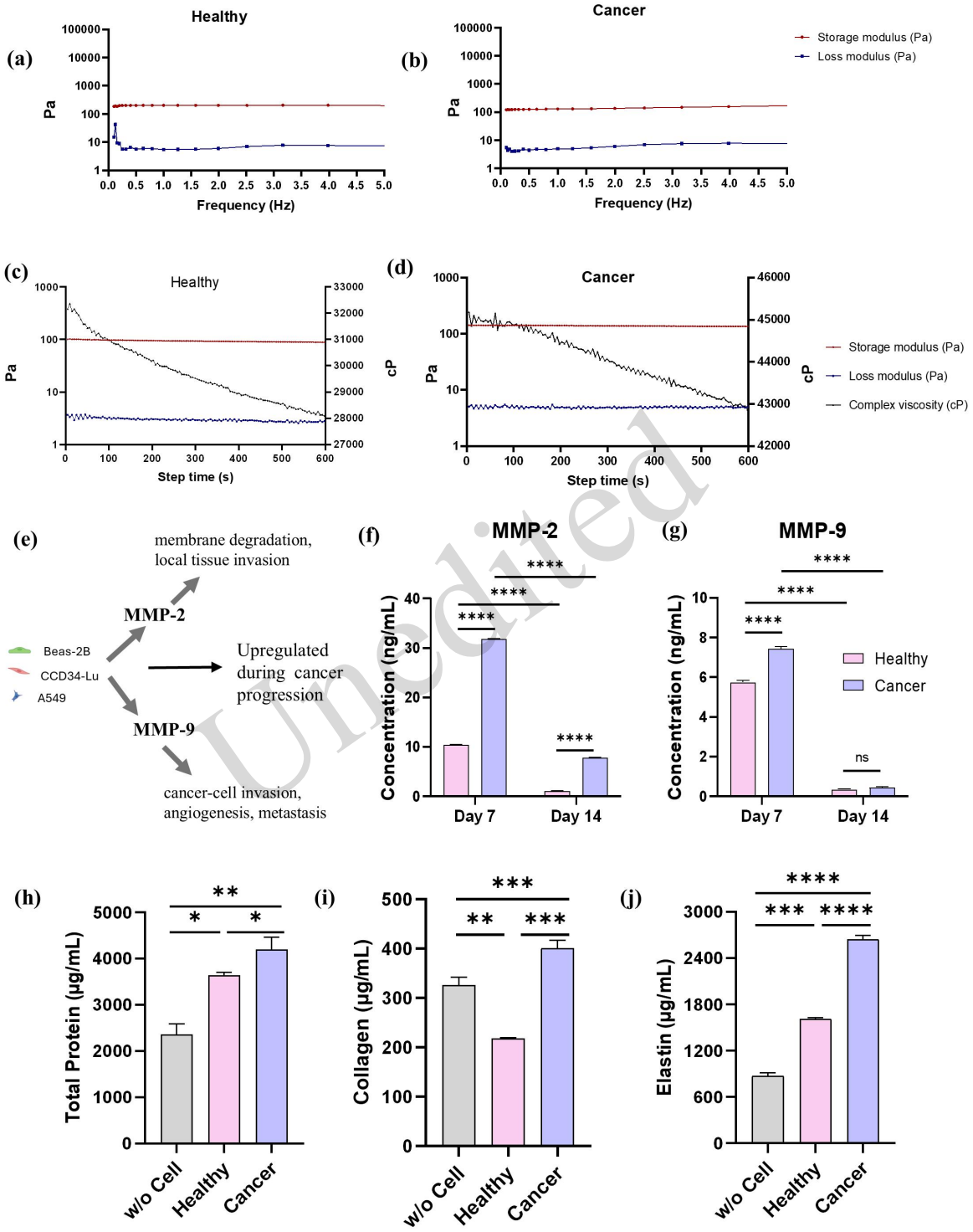

Fig. 4. Investigation of the effect of lung cancer on LME by biochemical and rheological analysis. Frequency-sweep plots of (a) healthy and (b) tumor models. Loss and storage modulus, viscosity plots of (c) healthy and (d) tumor models, (e) Schematic representation of MMP-2 and MMP-9 regulation during cancer progression, (f) MMP-2 and (g) MMP-9 expression plots of healthy and tumor models, (h) total protein, (i) collagen and (j) elastin content of cell-free, healthy, and tumor models). Data are expressed as mean±standard deviation (SD) (n=3). Error bars represent standard deviation, sd (ns, no significance, *P<0.05, **P<0.01, ***P<0.001,****P<0.0001). SM represents storage modulus, LM represents loss modulus, and w/o cell represents cell-free hydrogel.

Unedited

Matrix metalloproteinases (MMPs), particularly gelatinases such as MMP-2 and MMP-9, are critical effectors of ECM remodeling and are secreted by various stromal and epithelial cell types (Thomas et al., 2024; Filiz et al., 2024). These enzymes facilitate cancer-cell invasion, angiogenesis, and metastasis by degrading key structural ECM components such as collagen and laminin (Wolosowicz et al., 2024). MMP-2 is primarily involved in basement membrane degradation and local tissue invasion, while MMP-9 has been more closely associated with metastatic distribution in lung cancer **(Fig. 4e) (**Jabłońska-Trypuć et al., 2016; Merchant et al., 2017; Mondal et al., 2020). In our tumor model, significantly elevated expression of both enzymes was observed compared to the healthy model. MMP-2 levels reached 31.83 ± 0.1 ng/mL on day 7 and decreased to 7.84 ± 0.05 ng/mL by day 14, whereas the healthy model showed a decrease from 10.41 ± 0.1 ng/mL to 1.09 ± 0.01 ng/mL over the same period **(Fig. 4f)**. Similarly, MMP-9 levels in the tumor model downregulated from 7.4 ± 0.1 ng/mL to 0.45 ± 0.04 ng/mL, while the healthy model exhibited a decrease from 5.72 ± 0.2 ng/mL to 0.34 ± 0.04 ng/mL **(Fig. 4g)**. This result suggests an initial upregulation of MMPs in response to ECM-rich conditions, followed by reduced expression as degradation proceeded. To assess the biochemical outcomes of our remodeling, we quantified ECM protein content across experimental groups. Total protein was highest in the cancer group (4200.74 ± 267.2 μg/mL), followed by the healthy (3634.07 ± 73.3 μg/mL) and cell-free (2360 ± 230.5 μg/mL) groups (**Fig. 4h**). Notably, collagen levels were elevated in both the cancer (400.80 ± 15.9 μg/mL) and cell-free (326.48 ± 15.5 μg/mL) groups relative to the healthy model (218.56 ± 1.3 μg/mL), potentially due to tumor-induced matrix expression **(Fig. 4i)**. Elastin followed a similar trend, with the highest content in the cancer model (2644.40 ± 49.8 μg/mL), moderate levels in the healthy model (1612.07 ± 17.1 μg/mL), and the lowest levels in the cell-free model (872.84 ± 43.7 μg/mL) **(Fig. 4j)**. The observed increase in both MMP levels (on day 7) and ECM components such as collagen and elastin in this study could be attributed to a mechanism in which tumor-associated remodeling results in localized matrix stiffening and potentially stimulates MMP secretion via mechanotransductive signaling pathways such as integrin-FAK-YAP/TAZ (Ishihara and Haga, 2022). This interaction demonstrates the complex environment of matrix remodeling in lung cancer, in which MMPs not only degrade the ECM but also actively regulate the biochemical and mechanical architecture of the TME (Siddhartha and Garg, 2023; Zhang et al., 2023).

Uncorrected

4 Conclusions

In summary, this study successfully demonstrates the optimization and application of decellularized lung-tissue-derived ECM combined with GelMA as a hybrid gel to mimic the LME and TME in a 3D *in vitro* model. By optimizing decellularization protocols, we effectively removed cellular components while preserving key ECM proteins, including collagen, elastin, and glycosaminoglycans, which are critical for maintaining the structural and functional characteristics of lung tissue. The dlECM hydrogel, combined with GelMA, provided a suitable matrix for cell growth and proliferation, with 75% GelMA-25% dlECM hydrogel showing the highest cell viability. We tried to form a droplet structure, which successfully mimics the tumor form in the LME and demonstrates how the tumor's presence influences ECM remodeling and cell behavior. Rheological analysis revealed that the tumor model exhibits a significantly higher SM compared to the healthy model, reflecting the increased stiffness associated with cancer progression and ECM remodeling. The elevated levels of MMP-2 and MMP-9 in the cancer model further support the concept of active degradation of the ECM, a process essential for tumor invasion and metastasis. Also, the elevated levels of total protein, collagen, and elastin in the cancer model reflect active ECM remodeling associated with tumor progression. The fluorescence images confirm that lung-cancer cells (A549) actively invade from the tumor focus into the surrounding microenvironment, while healthy lung cells (BEAS-2B and CCD34-Lu) proliferated in the healthy model.

Overall, this study highlights the potential of using decellularized ECM-based hydrogels as a versatile, cost-effective, and reproducible platform for studying tumor biology and cell-ECM interactions, and for testing therapeutic strategies; ideally providing a more accurate and physiologically relevant model for cancer research and other applications.

Data availability statement

Acknowledgments

This work is supported by the Health Institutes of Turkiye (36064).

Author contributions

Aysel SASKARA and Yagmur ARSLAN performed the experimental research and data analysis, wrote and edited the manuscript. Ozlem YESIL-CELIKTAS contributed to the study design, data analysis, writing and editing of the manuscript. All authors read and approved the final manuscript and, therefore, had full access to all the data in the study and take responsibility for the integrity and security of the data.

Compliance with ethics guidelines

Aysel SASKARA,Yagmur ARSLAN and Ozlem YESIL-CELIKTAS declare that they have no conflict of interest.

References

Ashja Ardalan, A., Khalili-Tanha, G., et al., 2024. Shaping the landscape of lung cancer: the role and therapeutic potential of matrix metalloproteinases. *Int. J. Transl. Med.*, 4(4):661–679. http://dx.doi.org/10.3390/ijtm4040046

Bartnikowski, M., Wellard, R.M., Woodruff, M., et al., 2015. Tailoring hydrogel viscoelasticity with physical and chemical crosslinking. *Polymers*, 7(12):2650-2669. http://dx.doi.org/10.3390/polym7121539

Blanco-Fernandez, B., Gaspar, V.M., et al., 2021. Proteinaceous hydrogels for bioengineering advanced 3D tumor models. *Adv. Sci.*, 8(4):2003129. http://dx.doi.org/10.1002/advs.202003129

Cakmak, B., Saglam-Metiner, P., et al., 2022. A 3D in vitro co-culture model for evaluating biomaterial-mediated modulation of foreign-body responses. *Bio-Des. Manuf.*, 5(3):465–480. http://dx.doi.org/10.1007/s42242-022-00198-z

Das, P., Singh, S., et al., 2020. Tissue-derived decellularized extracellular matrices toward cartilage repair and regeneration. In: Methods in Cell Biology, Vol. 157, pp. 185–221. *Academic Press*. http://dx.doi.org/10.1016/bs.mcb.2019.11.005

Devamoglu, U., Arslan, Y., et al., 2025. Dual role of electrical stimulation and extracellular matrix on neural differentiation through the biomimetic interface. *Biomater. Sci.*, 13:3707–3721. https://doi.org/10.1039/D4BM01702

Edgar-Vilar, H., Correia, F.P., de Carvalho, M.T., et al., 2025. Biomimicking tissue microenvironments via decellularized mat rix-polymer combinations. *Adv Polym Life Sci*, p.43-75. http://dx.doi.org/10.1142/14148

Elosegui-Artola, A., Gupta, M., et al., 2023. Matrix viscoelasticity controls spatiotemporal tissue organization. *Nat. Mater.*,

Unedited

22(1):117–127.

http://dx.doi.org/10.1038/s41563-022-01400-4

Esch, E.W., Bahinski, A., et al., 2015. Organs-on-chips at the frontiers of drug discovery. *Nat. Rev. Drug Discov.*, 14(4):248–260.

http://dx.doi.org/10.1038/nrd4539

Evje, S., Waldeland, J.O., 2019. How tumor cells can make use of interstitial fluid flow in a strategy for metastasis. *Cell. Mol. Bioeng.*, 12(3): 227–254.

http://dx.doi.org/10.1007/s12195-019-00569-0

Fanjul-Fernández, M., et al., 2013. Matrix metalloproteinase Mmp-1a is dispensable for normal growth and fertility in mice and promotes lung cancer progression by modulating inflammatory responses. *J Biol Chem*, 288:14647-14656. http://dx.doi.org/10.1074/jbc.M112.439893

Ferreira, L.P., Gaspar, V.M., et al., 2020. Decellularized extracellular matrix for bioengineering physiomimetic 3D in vitro tumor models. *Trends Biotechnol.*, 38(12):1397–1414.

http://dx.doi.org/10.1016/j.tibtech.2020.04.006

Filiz, Y., Arslan, Y., Duran, E., et al., 2024. Decellularized plant-derived vasculature-on-a-chip interacting with breast cancer spheroids to evaluate a dual-drug therapy. *Appl Mater Today*, 36:102015.

http://dx.doi.org/10.1016/j.apmt.2023.102015

Firatligil-Yildirir, B., Bati-Ayaz, G., Nonappa, et al., 2024. Invasion/chemotaxis-and extravasation-chip models for breast cancer bone metastasis. *PLoS One,* 19(10):e0309285.

http://dx.doi.org/10.1371/journal.pone.0309285

Fu, Y., Fan, X., Tian, C., et al., 2016. Decellularization of porcine skeletal muscle extracellular matrix for the formulation of a matrix hydrogel: a preliminary study. *J Cell Mol Med*, 20(4):740-749.

http://dx.doi.org/10.1111/jcmm.12776

Gilbert, S.J., Bonnet, C.S., Blain, E.J., 2021. Mechanical cues: bidirectional reciprocity in the extracellular matrix drives mec hano-signalling in articular cartilage. *Int J Mol Sci*, 22(24):13595.

http://dx.doi.org/10.3390/ijms222413595

Herbst, R.S., Morgensztern, D., et al., 2018. The biology and management of non-small cell lung cancer. *Nature*, 553(7689):446–454.

http://dx.doi.org/10.1038/nature25183

Hocevar, S.E., Liu, L., Duncan, R.K., 2021. Matrigel is required for efficient differentiation of isolated, stem cell-derived otic vesicles into inner ear organoids. *Stem Cell Res,* 53:102295.

http://dx.doi.org/10.1016/j.scr.2021.102295

Inci, I., Norouz Dizaji, A., Ozel, C., et al., 2020. Decellularized inner body membranes for tissue engineering: a review. *J Biomater Sci Polym Ed*, 31(10):1287-1368.

http://dx.doi.org/10.1080/09205063.2020.1751523

Ishihara, S., Haga, H., 2022. Matrix stiffness contributes to cancer progression by regulating transcription factors. *Cancers*,

Unedited

14(4):1049.
http://dx.doi.org/10.3390/cancers14041049

Jabłońska-Trypuć, A., Matejczyk, M., Rosochacki, S., 2016. Matrix metalloproteinases (MMPs), the main extracellular matrix (ECM) enzymes in collagen degradation, as a target for anticancer drugs. *J Enzyme Inhib Med Chem*, 31(sup1):177-183.
http://dx.doi.org/10.3109/14756366.2016.1161620

Karamanos, N.K., Theocharis, A.D., et al., 2021. A guide to the composition and functions of the extracellular matrix. *The FEBS Journal*, 288(24):6850–6912.
http://dx.doi.org/10.1111/febs.15776

Kaya, B., Yesil-Celiktas, O., 2024. Ionic liquid-based transparent membrane-coupled human lung epithelium-on-a-chip de monstrating PM0.5 pollution effect under breathing mechanostress. *Bio-Des. Manuf.*, 7(5):624-636.
http://dx.doi.org/10.1007/s42242-024-00289-z

Kleinman, H.K., Martin, G.R., 2005. Matrigel: basement membrane matrix with biological activity. *Semin Cancer Biol,* 15(5):378-386.
http://dx.doi.org/10.1016/j.semcancer.2005.05.004

Kort-Mascort, J., Bao, G., Elkashty, O., et al., 2021. Decellularized extracellular matrix composite hydrogel bioinks for the de velopment of 3D bioprinted head and neck in vitro tumor models. *ACS Biomater Sci Eng*, 7(11):5288-5300.
http://dx.doi.org/10.1021/acsbiomaterials.1c00812

Kuşoğlu, A., Yangın, K., Özkan, S.N., et al., 2023. Different decellularization methods in bovine lung tissue reveals distinct biochemical composition, stiffness, and viscoelasticity in reconstituted hydrogels. *ACS Appl Bio Mater*, 6(2):793-805.
http://dx.doi.org/10.1021/acsabm.2c00968

Li, N., Zhang, W., et al., 2019. Analysis of cellular biomolecules and behaviors using microfluidic chip and fluorescence method. *Trends Anal. Chem.*, 117:200–214.
http://dx.doi.org/10.1016/j.trac.2019.05.029

Lim, K.S., Klotz, B.J., Lindberg, G.C.J., et al., 2019. Visible light cross-linking of gelatin hydrogels offers an enhanced cell microenvironment with improved light penetration depth. *Macromol Biosci,* 19(6):e1900009.
http://dx.doi.org/10.1002/mabi.201900098

Mao, B.H., Thi, K.M.N., Tang, M.J., et al., 2023. The interface stiffness and topographic feature dictate interfacial invasiveness of cancer spheroids. *Biofabrication*, 15(1):015023.
http://dx.doi.org/10.1088/1758-5090/acaa00

Merchant, N., Nagaraju, G.P., Rajitha, B., et al., 2017. Matrix metalloproteinases: their functional role in lung cancer. *Carcino genesis,* 38(8):766-780.
http://dx.doi.org/10.1093/carcin/bgx063

Miri, A.K., Hosseinabadi, H.G., Cecen, B., et al., 2018. Permeability mapping of gelatin methacryloyl hydrogels. *Acta Biomate rialia*, 77: 38–47.
http://dx.doi.org/10.1016/j.actbio.2018.07.006

Unedited

Mishra, D.K., Sakamoto, J.H., et al., 2012. Human lung cancer cells grown in an ex vivo 3D lung model produce matrix metal loproteinases not produced in 2D culture. http://dx.doi.org/10.1371/journal.pone.0045308

Moffat, D., Ye, X., et al., 2022. Decellularization for the retention of tissue niches. *J. Tissue Eng.*, 13:20417314221101151. http://dx.doi.org/10.1177/2041731422110115

Mondal, S., Adhikari, N., Banerjee, S., et al., 2020. Matrix metalloproteinase-9 (MMP-9) and its inhibitors in cancer: a minire view. *Eur J Med Chem,* 194:112260. http://dx.doi.org/10.1016/j.ejmech.2020.112260

Munson, J.M., Shieh, A.C., 2014. Interstitial fluid flow in cancer: implications for disease progression and treatment. *Cancer Manag Res*, 6: 317–328. http://dx.doi.org/10.2147/CMAR.S65444

Ohata, K., Ott, H.C., 2020. Human-scale lung regeneration based on decellularized matrix scaffolds as a biologic platform. *Surg Today,* 50:633-643. http://dx.doi.org/10.1007/s00595-020-02000-y

O'Neill, J.D., Anfang, R., Anandappa, A., et al., 2013. Decellularization of human and porcine lung tissues for pulmonary tissue engineering. *Ann Thorac Surg*, 96(3):1046-1056. http://dx.doi.org/10.1016/j.athoracsur.2013.04.022

Oyen, M.L., 2014. Mechanical characterisation of hydrogel materials. *Int Mater Rev*, 59(1):44-59. http://dx.doi.org/10.1179/1743280413Y.0000000022

Özdinç, Ş., Sarıca, S., Özkan, S.N., et al., 2023. Development and characterization of decellularized lung extracellular matrix hydrogels. *J. Vis. Exp.*, (202):e65768. http://dx.doi.org/10.3791/65768

Parvin, N., Kumar, A., et al., 2024. Cutting-Edge Hydrogel Technologies in Tissue Engineering and Biosensing: An Updated Review. *Materials*, 17(19):4792. http://dx.doi.org/10.3390/ma17194792

Phogat, S., Thiam, F., Al Yazeedi, S., et al., 2023. 3D in vitro hydrogel models to study the human lung extracellular matrix and fibroblast function. *Respir Res*, 24(1):242. http://dx.doi.org/10.1186/s12931-023-02548-6

Poon, C., 2022. Measuring the density and viscosity of culture media for optimized computational fluid dynamics analysis of in vitro devices. *J. Mech. Behav.*, 126: 105024. http://dx.doi.org/10.1016/j.jmbbm.2021.105024

Rahman, Z., Bordoloi, A.D., Rouhana, H., et al., 2024. Interstitial flow potentiates TGF-β/Smad-signaling activity in lung cancer spheroids in a 3D-microfluidic chip. *Lab Chip*, 24(3): 422–433. http://dx.doi.org/10.1039/D3LC00886J

Unedited

Saldin, L.T., Cramer, M.C., et al., 2017. Extracellular matrix hydrogels from decellularized tissues: Structure and function. *Acta Biomater*, 49:1–15.
http://dx.doi.org/10.1016/j.actbio.2016.11.068

Saraswathibhatla, A., Indana, D., et al., 2023. Cell–extracellular matrix mechanotransduction in 3D. *Nat. Rev. Mol. Cell Biol.*, 24(7):495–516.
http://dx.doi.org/10.1038/s41580-023-00583-1

Saygili, E., Devamoglu, U., et al., 2023. An optical pH-sensor integrated microfluidic platform multilayered with bacterial cel lulose and gelatin methacrylate to mimic drug-induced lung injury. *J. Ind. Eng. Chem.* ,121:190–199.
http://dx.doi.org/10.1016/j.jiec.2023.01.023

Sicari, B.M., Londono, R., Badylak, S.F., 2014. Extracellular matrix as a bioscaffold for tissue engineering. In: Badylak, S.F. (Ed.), Tissue Engineering, 2nd ed. *Academic Press*, p.149-175.
http://dx.doi.org/10.1016/B978-0-12-824459-3.00005-6

Siddhartha, R., Garg, M., 2023. Interplay between extracellular matrix remodeling and angiogenesis in tumor ecosystem. *Mol Cancer Ther*, 22(3):291-305.
http://dx.doi.org/10.1158/1535-7163.MCT-22-0595

Tao, M.H., 2019. Epidemiology of lung cancer. Lung Cancer and Imaging. *IOP Publishing.*
https://doi.org/10.1088/978-0-7503-2540-0ch4

Thakor, J., Ahadian, S., et al., 2020. Engineered hydrogels for brain tumor culture and therapy. *Bio-Des. Manuf.*, 3:203–226.
http://dx.doi.org/10.1007/s42242-020-00084-6

Thomas, J.T., Joseph, B., Waltimo, T., 2024. Matrix metalloproteinases (MMPs). In: Sorsa, T. (Ed.), Advances in Gingival Di seases and Conditions. *Springer*, p.37.

Trębacz, H., Barzycka, A., 2023. Mechanical properties and functions of elastin: an overview. *Biomolecules*, 13(3):574.
http://dx.doi.org/10.3390/biom13030574

Valdoz, J.C., Johnson, B.C., Jacobs, D.J., et al., 2021. The ECM: to scaffold, or not to scaffold, that is the question. *Int J Mol Sci*, 22(23):1269.
http://dx.doi.org/10.3390/ijms222312690

Wang, L., Hu, D., Xu, J., et al., 2024. Complex in vitro model: A transformative model in drug development and precision me dicine. *Clin Transl Sci*, 17(2):e13695.
http://dx.doi.org/10.1111/cts.13695

Wang, X., Chan, J., et al., 2022. Decellularized blood vessel development: Current state-of-the-art and future directions. *Front. bioeng. Biotechnol.*, 10:951644.
http://dx.doi.org/10.3389/fbioe.2022.95164

Wang, Y., Song, E.C., Resnick, M.B., 2020. Elastin in the tumor microenvironment. In: Karamanos, N.K. (Ed.), Tumor Micro environment: Extracellular Matrix Components-Part B. *Springer*, p.1-16.
http://dx.doi.org/10.1007/978-3-030-48457-6_1

Unedited

Wolosowicz, M., Prokopiuk, S., Kaminski, T.W., 2024. The complex role of matrix metalloproteinase-2 (MMP-2) in health and disease. *Int J Mol Sci*, 25(24):13691. http://dx.doi.org/10.3390/ijms252413691

Xie, W., Wei, X., Kang, H., et al., 2023. Static and dynamic: evolving biomaterial mechanical properties to control cellular mechanotransduction. *Adv Sci,* 10(9):2204594. http://dx.doi.org/10.1002/advs.202204594

Yaldiz, B., Saglam-Metiner, P., Cam, S.B., et al., 2021a. Effect of sterilization methods on the mechanical stability and extra cellular matrix constituents of decellularized brain tissue. *J Supercrit. Fluids*, 175:105299. http://dx.doi.org/10.1016/j.supflu.2021.10529

Yaldiz, B., Saglam-Metiner, P., Yesil-Celiktas, O., 2021b. Decellularised extracellular matrix-based biomaterials for repair and regeneration of central nervous system. *Expert Rev. Mol. Med.*, 23:e25. http://dx.doi.org/10.1017/erm.2021.22

Yildiz-Ozturk, E., Saglam-Metiner, P., Yesil-Celiktas, O., 2021. Lung carcinoma spheroids embedded in a microfluidic platform. *Cytotechnology*, 73(3):457–471. http://dx.doi.org/10.1007/s10616-021-00470-7

Yue, K., Trujillo-de Santiago, G., Alvarez, M.M., et al., 2015. Synthesis, properties, and biomedical applications of gelatin met hacryloyl (GelMA) hydrogels. *Biomaterials*, 73:254-271. http://dx.doi.org/10.1016/j.biomaterials.2015.08.045

Zhang, Y., Wang, Y., Li, Y., et al., 2023. Application of collagen-based hydrogel in skin wound healing. *Gels*, 9(3):185. http://dx.doi.org/10.3390/gels9030185

Zhu, S., Yuan, Q., Yin, T., et al., 2018. Self-assembly of collagen-based biomaterials: preparation, characterizations and biome dical applications. *J Mater Chem B*, 6(18):2650-2676. http://dx.doi.org/10.1039/C7TB02999C

Supplementary information

Figs. S1-S2; Results and discussion

Unedited